ACS Partner Journal

Journal of the American Society for Mass Spectrometry

pubs.acs.org/jasms

Article

Structural Characterization of Dimeric Perfluoroalkyl Carboxylic Acid Using Experimental and Theoretical Ion Mobility Spectrometry Analyses

Aurore Schneiders, Johann Far, Lidia Belova, Allison Fry, Adrian Covaci, Erin S. Baker, Edwin De Pauw, and Gauthier Eppe*

Cite This: https://doi.org/10.1021/jasms.5c00007

Read Online

ACCESS | Metrics & More | Article Recommendations | Supporting Information

ABSTRACT: Per- and polyfluoroalkyl substances (PFAS) are contaminants of increasing concern, with over seven million compounds currently inventoried in the PubChem PFAS Tree. Recently, ion mobility spectrometry has been combined with liquid chromatography and high-resolution mass spectrometry (LC-IMS-HRMS) to assess PFAS. Interestingly, using negative electrospray ionization, perfluoroalkyl carboxylic acids (PFCAs) form homodimers ($[2M-H]^-$), a phenomenon observed with trapped, traveling wave, and drift-tube IMS. In addition to the limited research on their effect on analytical performance, there is little information on the conformations these dimers can adopt. This study aimed to propose most probable conformations for PFCA dimers. Based on qualitative analysis of how collision cross section (CCS) values change with the mass-to-charge ratio (m/z) of PFCA ions, the PFCA dimers were hypothesized to likely adopt a V-shaped structure. To support this assumption, *in silico* geometry optimizations were performed to generate a set of conformers for each possible dimer. A CCS value was then calculated for each conformer using the trajectory method with Lennard-Jones and ion-quadrupole potentials. Among these conformers, at least one of the ten lowest-energy conformers identified for each dimer exhibited theoretical CCS values within a ±2% error margin compared to the experimental data, qualifying them as plausible structures for the dimers. Our findings revealed that the fluorinated alkyl chains in the dimers are close to each other due to a combination of C−F···O=C and C−F···F−C stabilizing interactions. These findings, together with supplementary investigations involving environmentally relevant cations, may offer valuable insights into the interactions and environmental behavior of PFAS.

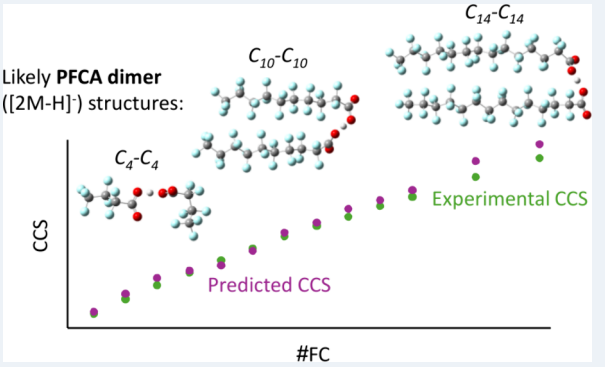

INTRODUCTION

Per-and polyfluoroalkyl substances (PFAS) are a group of molecules containing at least one fully fluorinated carbon atom (either $-CF_3$ or $-CF_2-$).[1] Since the 1950s, they have been widely used in industrial and commercial applications due to their specific properties, such as grease and water repellency as well as thermal resistance.[2−4] However, because of their inherent stability and extensive use, these compounds are found and prevail in many environmental matrices. Since toxicological studies have linked PFAS exposure to a variety of health issues,[3,5] many concerns have been raised about the ubiquitous presence. In response to growing concerns about long-chain perfluoroalkyl carboxylic acids (PFCAs) and perfluoroalkyl sulfonic acids (PFSAs),[6] major manufacturers voluntarily discontinued production of these substances, their salts, and related compounds, in the early 2000s.[2,7] As a result, alternative PFAS have emerged on the market.[8] Nevertheless, these alternative PFAS may not be any less persistent, toxic or bioaccumulative than the legacy PFAS they replace.[9−11] This underscores the urgent need for large-scale suspect and nontargeted screening methods to identify these substances.[9,12]

Currently, most approaches analyzing PFAS rely on reverse-phase liquid chromatography (RPLC) coupled with high resolution mass spectrometry (HRMS).[9,10,12,13] However, the identification of emerging PFAS remains challenging due to the numerous different classes of PFAS, with various functional groups, potential presence of numerous isobars or isomers,[10,14] as well as the limited availability of analytical standards.[10] In this regard, the coupling of ion mobility spectrometry (IMS) with conventional LC-HMRS setups has been introduced to offer new perspectives for PFAS analyses.[12,14−16] IMS is a fast

Received: January 6, 2025
Revised: February 14, 2025
Accepted: February 21, 2025

separation tool, acting in the millisecond range, which can differentiate ions based on their charge, and gas-phase size and shape.[14−18] Briefly, ions are accelerated by an electric field against a buffer gas and separated based on their mobility under these conditions.[17,18] The time scale of IMS is compatible with chromatographic separation (on the order of seconds) and time-of-flight mass analyzers (TOF-MS) (on the order of microseconds), thereby increasing peak capacity without increasing analysis time.[14−16] In addition, the collision cross-section (CCS) calculated from IMS data can be seen as a molecular descriptor related to the apparent bulk density of the gas-phase ions, providing an additional point of identification.[14,18,19] In the case of PFAS, CCS versus mass-to-charge ratio (CCS-m/z) trendlines are observed for homologous series, which can further enhance the confidence in identifying homologous PFAS.[14,20] A few studies have reported the analysis of PFAS using LC-IMS-HRMS with negative electrospray ionization (ESI),[14,16,20−24] primarily employing drift tube ion mobility spectrometry (DTIM). Two of these studies identified the presence of deprotonated PFCAs $[M\text{-}H]^-$, decarboxylated PFCAs $[M\text{-}H-CO_2]^-$ and dimeric forms of PFCAs ($[2M\text{-}H]^-$).[11,21] These dimeric species were also observed using traveling wave IMS (TWIMS).[23] In both cases, the LC mobile phase was buffered with ammonium acetate, and the injected solution contained PFCA concentrations ranging from 0.2 to 10 μg/mL. This dimer formation is therefore a characteristic of PFCAs, under the conditions of multiple different IMS configurations. This is corroborated by a study reporting that the hydrogen bond between the two carboxylate groups, which is responsible for PFOA homodimers formation, is particularly strong, as these dimers were still detectable at high acceleration potentials (i.e., 150 V).[25]

While these experimental studies have illustrated dimer presence, there is limited knowledge about the conditions under which PFAS dimers are formed or detected, and if it is dependent on the IMS setup employed. Furthermore, the proportion of dimers detected can significantly influence the sensitivity of the target analyte in negative mode studies.[10] Conversely, the presence of a dimeric ion can serve as an additional point of identification for the analyte.[21] Little, however, is known about possible conformations PFAS may adopt in the gas phase. Thus, understanding the conformation of these dimers could provide information on the environmental fate of PFAS[26] or their possible biological interactions.[27]

In this study, the CCS values for PFCA dimers (and monomers) were evaluated experimentally with three different IMS setups (DTIMS, TIMS and TWIMS). CCS values were obtained for homodimeric ions of the PFCA homologous series (spanning PFCAs with 4 to 18 carbon atoms), and the CCS versus m/z dimer trend was analyzed to infer structural information. CCS theoretical calculations were then employed to assess the PFCA dimer conformations.

EXPERIMENTAL SECTION

Chemicals. Initial LC-TIMS-TOF MS experiments to assess PFCA dimerization were conducted using a mixture of PFAS standards purchased from Wellington laboratories, Inc. (Guelph, Canada), under product code "PFAC-MXC". This mixture included C_4-C_{14}, C_{16}, and C_{18} PFCAs, and C_4-C_{10} and C_{12} PFSAs, at an initial concentration of 2 μg/mL. The mixture was then diluted to a final concentration of 0.1 μg/mL in methanol (99.9%, Biosolve). Additional individual PFCA analytical standards matching those in the mixture were obtained from Dr. Ehrenstorfer GmbH (Augsburg, Germany). Each PFCA standard was solubilized in methanol and diluted to a concentration of 10 μg/mL. For the direct injection (DI) DTIM study of $[2M\text{-}H]^-$ dimers, five solutions (300 ng/mL each) were prepared in MeOH by mixing pairs of PFCA standards: C_4+C_{14}, C_5+C_{13}, C_6+C_{12}, C_7+C_{11} and C_8+C_{10}. A 300 ng/mL solution of C_9 PFCA and 400 ng/mL solutions of C_{16} and C_{18} PFCAs were also prepared in methanol. A C_2+C_{16} solution was prepared by adding a TFA (trifluoroacetic) solution to the 400 ng/mL C_{16} PFCA solution, achieving a final TFA concentration of 100 ng/mL. These solutions enabled the detection of both heterodimeric and homodimeric species. For instance, the C_4+C_{14} solution allowed the detection of the C_4-C_4 and $C_{14}-C_{14}$ homodimers, as well as the C_4-C_{14} heterodimer. For the DI-TIMS and DI-TWIMS analysis of $[2M\text{-}H]^-$ dimers, the same 300 ng/mL or 400 ng/mL solutions were prepared in methanol containing 0.1% formic acid.

Instrumentation. Initial LC-TIMS-TOF MS experiments on the PFAC-MXC mixture were carried out using an Acquity I-Class UPLC system, coupled with a TIMSTOF Pro2 spectrometer (Bruker Daltonics, Bremen, Germany), equipped with an ESI source operated in negative mode. Chromatographic separation was performed using an Acquity BEH C_{18} column heated to 45 °C (2.1 × 150 mm × 1.7 μm particles) (Waters, Milford, MA, USA). The injection volume was 5 μL. The flow rate was 0.2 mL/min with a binary mobile phase gradient of water with 0.1% formic acid and acetonitrile (detailed conditions available in the Supporting Information (S.I.)). For DI-TIMS experiments, the 300 ng/mL and 400 ng/mL PFCA solutions were introduced directly into the ESI source at a flow rate of 5 μL/min via the integrated syringe pump of the TIMSTOF instrument.

Direct injection experiments on the 300 ng/mL and 400 ng/mL PFCA solutions were also conducted using the TWIMS SYNAPT G2 HDMS mass spectrometer (Manchester, UK) and the Agilent 6560 drift tube ion mobility quadrupole time-of-flight mass spectrometer (DTIM-QTOF) in negative ESI mode. PFCA solutions were injected directly using an Agilent 1290 Infinity II UPLC connected to the DTIM-QTOF, using an injection volume of 2 μL. The mobile phase consisted of methanol with 0.1% formic acid, at a flow rate of 0.2 mL/min. For TWIMS experiments, PFCA solutions were injected directly into the ESI source at a flow rate of 6 μL/min using a syringe pump. Calibration of CCS values for all three IMS instruments was carried out using low-concentration tune mixture (Agilent Technologies, Santa Clara, USA). Detailed experimental parameters, CCS calibration procedures, and data processing methods for each IMS setup can be found in the S.I. The reported CCS values obtained from DTIM and TIMS represent the average of five injections, whereas the CCS values reported for TWIMS are the average of three injections.

Theoretical Calculations of CCS Values. A comprehensive workflow was developed to explore a set of conformers for each PFCA dimeric ion (See result part for greater details). The process began with 15 distinct orientations of the two fluorinated chains relative to the proton. Additional conformers were generated through relaxed potential energy scans. These conformers were then optimized using density functional theory (DFT), with M06-2X functionals, employing the Gaussian 16 software package.[28] Following optimization, CCS values were predicted using the trajectory method imple-

https://doi.org/10.1021/jasms.5c00007
J. Am. Soc. Mass Spectrom. XXXX, XXX, XXX−XXX

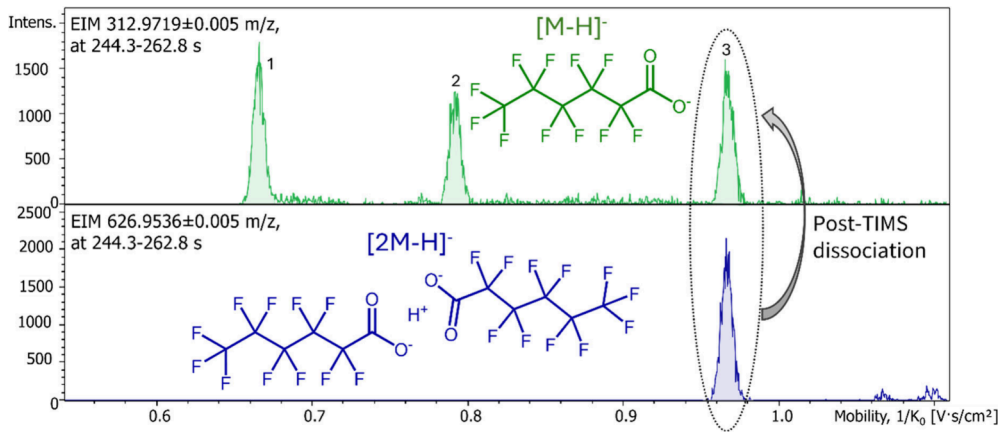

Figure 1. Extracted ion mobilograms (EIMs) of the deprotonated PFHxA ion (green upper trace) and of the dimeric PFHxA ion (blue lower trace). A 2D schematic of each ion is shown in the plots.

mented in IMoS software (version 1.13).[29] This method includes a 4−6−12 potential[30] and the inclusion of the ion quadrupole potential for nitrogen was considered. Finally, for each dimer, a Boltzmann-weighted (BW) average CCS value was computed based on the zero-point corrected energies of each optimized conformer.

RESULTS AND DISCUSSION

PFCA Dimer Formation in IMS. For the experimental analyses of the PFAS molecules, both monomers and dimers were assessed. Tables presenting the experimental and theoretical CCS values for both monomers and dimers are provided in the S.I.

The ionization of PFCAs in negative ESI mode can lead to the formation of homodimeric ions ($[2M-H]^-$). These ions were detected in LC-TIMS-TOF MS on the PFAC-MXC mixture, with some undergoing dissociation into their corresponding deprotonated ions ($[M-H]^-$) between the TIMS cell and the TOF mass analyzer.

This process, termed here as "post-TIMS dissociation", results in the detection of ions with the m/z of the $[M-H]^-$ ion but exhibiting the ion mobility of the $[2M-H]^-$ ion since they move through the IMS cell as dimers but break into monomers following mobility analysis. The consequence is a mobilogram showing several peaks for the deprotonated ion. Figure 1 illustrates this phenomenon for perfluorohexanoic acid (PFHxA). The upper and lower traces represent the mobilograms of the $[M-H]^-$ and $[2M-H]^-$ ions, respectively. The first peak, displaying the lowest inverse reduced ion mobility ($1/K_0$), corresponds to the monomeric form of the deprotonated ion, which has the lowest CCS value. The third peak, aligned with the mobility of the homodimeric ions, corresponds to $[M-H]^-$ ions generated via post-TIMS dissociation of the $[2M-H]^-$ ions. The second peak arises from post-TIMS dissociation of an adduct of the $[M-H]^-$ ion and trifluoroacetic acid.

As illustrated for PFHxA (Figure 1), the intensities of dimeric and monomeric ions are comparable. This dimer formation could therefore negatively affect the sensitivity of the analysis, but more quantitative studies are needed to confirm this. Furthermore, if these dimers undergo post-TIMS dissociation, as shown in Figure 1, they may complicate the identification process. Nevertheless, dimeric ions can also provide additional identification confidence, which is particularly useful when interferences coexist with the monomeric ions or when the monomeric ions are not observable due to excessive in-source fragmentation, while the dimeric ion remains stable enough to be observed. For example, in the case of C_4 PFCA, the monomeric ion was not detected, but its dimeric ion was observed.

This formation of dimeric PFCA ions is more likely attributed to their physicochemical properties,[10] rather than the ionization conditions or TIMS configuration. Similar observations were made using two other IMS instruments having DTIM and TWIMS cells. Additionally, in this study, a mobile phase containing formic acid was used, but dimer formation has also been observed when using a mobile phase buffered with ammonium acetate, as reported in the literature.[11,21,23] These findings suggest that dimer formation is a characteristic feature of these compounds, with minimal dependence on the mobile phase. CCS values for $[2M-H]^-$ PFCA ions were obtained with all three devices via direct injection of 300 ng/mL or 400 ng/mL PFCA solutions (see Experimental section), with no notable differences observed (within ±2%)[24,31] (Figure 2a). The same consistency was found for the monomeric ions (Figure 2b) (see Table S3 and S4 for the $[M-H]^-$ and $[2M-H]^-$ CCS values). This finding demonstrates that the CCS values for both monomeric and dimeric ions are reproducible across the three IMS setups, which is analytically relevant. The consistency of the CCS values and trendlines further suggests that the ion structures remain similar, regardless of the IMS instrument used.

Experimental CCS Trendlines and Initial Structural Hypotheses. To understand CCS versus m/z trendlines, the CCS for each observed monomer and dimer were plotted versus their number of fluorinated carbon atoms. In Figure 2 (a and b), the x-axis represents the number of fluorinated carbon atoms (#FC), which can be seen as the degree of polymerization (DP). For example, #FC is 5 for PFHxA $[M-H]^-$ ions and #FC is 10 for PFHxA $[2M-H]^-$ ions. These plots illustrate trendlines between CCS values and DP for monomeric and dimeric ions, which can be compared with previous homopolymers analyses.[32,33] These studies demonstrated that a power regression model can describe the relationship between CCS with DP, as shown in eq 1.

$$\Omega = A \cdot \mathrm{DP}^{pow} \quad (1)$$

Where Ω represents the CCS, DP represents the degree of polymerization (#FC in PFAS case), and A and pow are the fitting parameters.

https://doi.org/10.1021/jasms.5c00007
J. Am. Soc. Mass Spectrom. XXXX, XXX, XXX−XXX

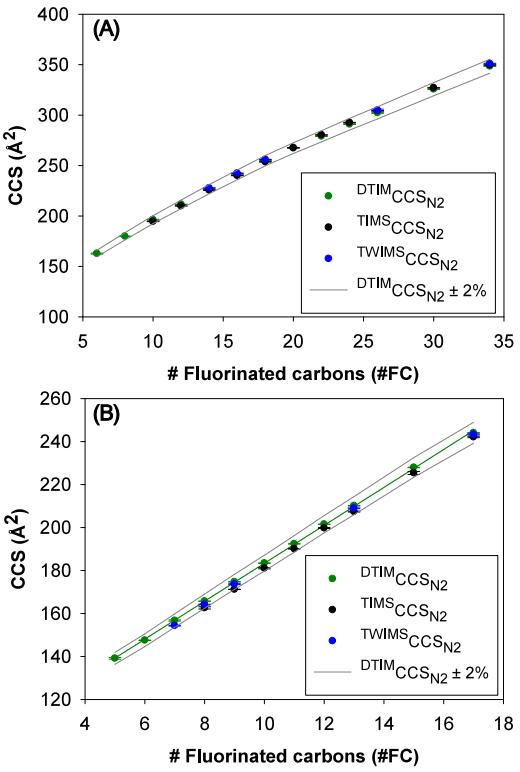

Figure 2. Comparison of CCS values obtained by DTIM, TIMS and TWIMS for dimeric (A) and monomeric (B) ions of PFCA. The *x*-axis represents the number of fluorinated carbons in the ions and the error bars represent twice the standard deviation, on five (DTIM, TIMS) or three (TWIMS) replicates.

The parameter *A* reflects the apparent density, as it accounts for the increase in CCS resulting from the addition of a repeating unit of a certain mean volume. A low value of *A* corresponds to a higher bulk density.[32] To gain insight into the likely structures of PFCA ions, the most relevant parameter is *pow*, which provides information about the general shapes of the ions.[33] Haler and co-workers have demonstrated that a *pow* value close to 2/3 implies a generally spherical shape growing isotropically, while a value near 1 indicates a cylindrical shape.

This linear relationship is observed for monomeric PFCA ions (Figure 2b), suggesting that the addition of a CF_2 unit (or FC) leads to ion growth in the form of a cylinder (Figure S1a), where the length increases but the diameter remains constant.

However, for dimeric ions, the evolution of CCS values with #FC is no longer linear and is better described using a power regression model, with a *pow* value of 0.45 when using eq 1. This indicates that the PFCA homodimers no longer adopt a cylindrical shape but may instead form a V-shaped structure with the proton connecting the two carboxylate ends (Figure S1b). This raises the question of the angle between the two fluorinated chains in these dimers. Since the *pow* factor is different from 2/3, the overall shape of the dimers is unlikely to be spherical (Figure S1c). To investigate this, several mixtures of two PFCA homologues capable of forming isomeric dimers, such as C_4+C_{14} (i.e., 3 FC + 13 FC), C_5+C_{13} and C_8+C_{10}, were analyzed by direct injection (DI), to promote the formation of the corresponding heterodimers (e.g., C_4−C_{14}). The rationale was as follows: if the PFCA dimers were spherical, similar CCS values would be expected regardless of asymmetry, because their overall shape would be equally compact and globular. However, the CCS were found to differ (Figure 3; see Table S5 for the values), showing a consistent trend across all IMS devices used (DTIM, TWIMS, or TIMS). Specifically, CCS decreased as the asymmetry of the dimers decreased. This observation effectively rules out the possibility of spherical $[2M\text{-}H]^-$ PFCA ions. Moreover, the similar trend observed across all three IMS setups reinforces the idea that the structural differences between these asymmetrical dimers are consistent, regardless of the IMS device employed.

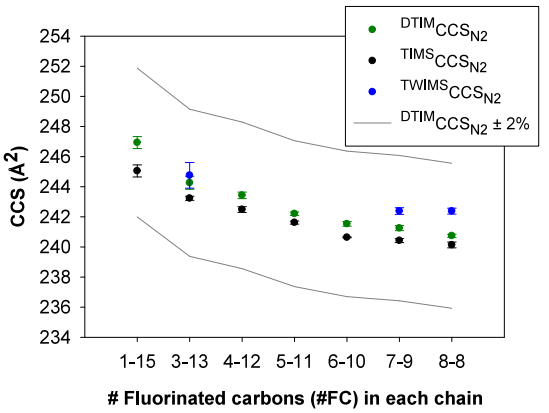

Figure 3. Comparison of CCS values obtained by DTIM, TIMS and TWIMS for asymmetrical and isomeric dimeric ions of PFCA. The *x*-axis represents the association between fluorinated carbons numbers in the two PFCA forming the dimer. The error bars represent twice the standard deviation, on five (DTIM, TIMS) or three (TWIMS) replicates.

According to this analysis of CCS versus *m*/*z* trendlines, PFCA monomeric ions are expected to have a cylindrical shape, while dimeric ions are neither cylindrical nor spherical. The most likely alternative is an intermediate structure, potentially a V-shape, for these dimers. These hypotheses were further explored using *in silico* CCS assessments. The aim was to develop a computational workflow for predicting the CCS of the dimeric ions to reproduce experimental CCS trendlines and provide insight into the plausible structure of PFCA dimers.

Quantum Chemistry-Based Predictions of Dimer Structures. To assess potential PFCA structures for comparison to experimental studies, first a set of conformers must be generated and optimizated, and their CCS values calculated. A final CCS value is then reported, based on an appropriate averaging method.[34−37] The following sections describe the implementation of a theoretical workflow for PFCA dimer analyses. This workflow was first tested and validated on monomeric ions before being applied to the dimeric ions.

Conformer Generation and Optimization for Dimeric Ions. In the case of the PFCA dimers studied, the first challenge is the generation of conformers. In the literature, this process is frequently carried out using molecular dynamics (MD) simulations, which rely on parametrized force fields such as MM2,[29] MMFF94[37] or Generalized Amber Force Field (GAFF).[34,36] However, these force fields are not well suited for modeling noncovalent proton bonding, as they do not (adequately) describe the proton (H^+). In addition, they may not be properly parametrized for PFAS-type molecules with multiple fluorine atoms. As a result, conformer generation via MD could lead to inaccurate starting geometries for PFCA

https://doi.org/10.1021/jasms.5c00007
J. Am. Soc. Mass Spectrom. XXXX, XXX, XXX−XXX

dimers. Thus, an alternative strategy for generating conformers had to be implemented. The workflow for conformer generation and CCS calculation for dimers is summarized in Figure 4.

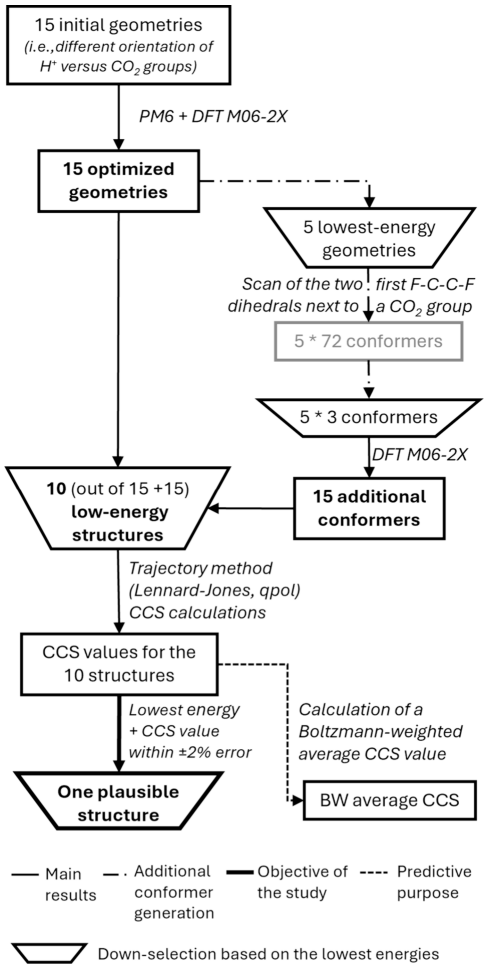

Figure 4. Workflow for conformer generation and CCS calculations for PFCA dimeric ions.

To minimize bias from initial assumptions, 15 different starting geometries (see Figure S2) were optimized for each dimer. The starting geometries were constructed by considering two linear fluorinated chains with varying positions relative to the proton. In some cases, the two fluorinated chains are positioned opposite each other, while in others, they are parallel, to sample a broad range of possible orientations. For each dimer, the same 15 initial chain orientations were used, but the lengths of the fluorinated chains were modified to represent the experimental molecules. These geometries were then preoptimized using the PM6 semiempirical method to ensure a plausible structure for the dimers. This semiempirical method was chosen because it has been shown to provide a reliable first approximation for PFAS structures[38] and hydrogen bonds.[39] The resulting geometries were then optimized using DFT calculations with the M06-2X functional at the 6-31+G(d,p) level at 298.15 K. To accurately predict the geometries and energies of PFCA dimeric ions, it is essential to use a function that properly accounts for long-range interactions, such as hydrogen bonds and F−F interactions. The M06-2X functional is well-suited for this purpose, as it includes long-range interactions and has been demonstrated to accurately describe noncovalent interactions,[40] predict the thermostability of PFCA[41] and PFSA[42] isomers, and determine the pK_a values of PFAS.[43]

After optimizing the 15 initial geometries, the five with the lowest energies were selected for relaxed potential energy scans to sample the conformational space and potentially identify low energy conformers. The first F−C−C−F dihedral angle adjacent to the CO_2 group of one of the chains (the longest in the case of asymmetrical dimers) was scanned with 36 steps of 10° each, using the M06-2X/6-31+G(d,p) level of theory. Subsequently, the second F−C−C−F dihedral angle was scanned on the local minimum structure identified from the previous scan. It was observed that further analysis of other dihedrals did not yield lower energy conformers; therefore, no additional dihedrals were scanned. From the 72 conformers generated for each geometry, three of the lowest-energy conformers, which were sufficiently distinct, were selected for reoptimization and frequency calculations at the same level of theory used for the scans. Finally, out of the 30 optimized conformers obtained, the ten lowest-energy conformers without imaginary frequency were selected for CCS prediction. In addition, if a dimer yielded a conformer with both the lowest energy and a consistent CCS value, its angles (dihedrals and $O_2C-H-CO_2$) were applied to the other dimers. If this conformer exhibited sufficiently low energy and a structure distinct from the previously identified conformers, it was included among the ten conformers used for CCS analysis.

Conformer Generation and Optimization for Monomeric Ions. The workflow described for dimers required slight adaptations for monomeric ions. This workflow is summarized in Figure S3. Redundant scan analyses were conducted at the M06-2X/6-31+G(d,p) level of theory. The analysis started with the F−C−C−F dihedral adjacent to the CO_2 part, followed by scanning the second F−C−C−F dihedral angle over the lowest-energetic conformer identified, and continuing similarly for subsequent dihedrals. This analysis showed that the dihedrals closest to the CO_2 group had the greatest influence on conformer energy, while those closer to the CF_3 tail were preferentially at around 155°−165°. Following these scans, seven distinct low-energy conformers were selected, along with the helical isomer (i.e., all dihedral angles around 165°). The selection was designed to ensure a diverse conformer set: at least two conformers with one dihedral angle less than 165°, three conformers with two dihedrals less than 165°, and for longer monomeric ions, at least one conformer with three dihedrals less than 165°. The selected conformers were then reoptimized at the M06-2X/6-31+G-(d,p) level of theory and used for CCS analysis.

Theoretical CCS Calculation. Theoretical CCS calculations were performed using the trajectory method (TM), regarded as the most rigorous approach.[17,35] The TM method used was implemented in IMoS (version 1.13), and employed 4−6−12 Lennard-Jones (LJ) potentials[44,45] supplemented by an additional ion-quadrupole potential to study ion mobility in N_2.[35] Previous studies have demonstrated that adding this ion-quadrupole interaction considerably enhances the agreement between experimental and theoretical CCS values for carboxylic acids anions.[32] Consequently, it can be reasonably assumed that a similar improvement would apply to dimeric PFCA ions. For the calculations, Mulliken and Natural Bond Orbital (NBO) atomic charge descriptions were tested. The number of gas molecules per orientation was 300,000 and the

https://doi.org/10.1021/jasms.5c00007
J. Am. Soc. Mass Spectrom. XXXX, XXX, XXX−XXX

gas temperature was set to 304 K, the default parameter. Note that none of the IM mass spectrometers used during this study were equipped with a gas temperature control in the IM cell section. Because the CCS values remained consistent across the three IMS setups, the ion effective temperature and the buffer gas temperature were assumed to be similar between the three instruments, which is generally accepted to be room temperature.[46] Therefore, the default temperature of 304 K was retained to compute the CCS values.

CCS Averaging Method. Once the CCS values were calculated for the ten lowest-energy structures (for dimers, Figure 4) or eight lowest-energy conformers (for monomers, Figure S3), a single CCS value needed to be obtained for predictive purposes. Reporting the CCS value of the lowest energy conformer may not always be relevant, as this conformer might not represent the global minimum. However, recent studies have shown that using a Boltzmann-weighted (BW) average CCS value offers greater accuracy.[34−37] This approach is also more representative of IMS experiments, as the reported CCS value reflects the weighted average of conformers based on their probability and lifetime within the IMS cell.[34,36] Boltzmann weighting was performed using zero-point corrected energies calculated by DFT[35] and the same temperature as the CCS calculations (304 K). Zero-point corrected energies were used, as they are expected to be less sensitive to approximation errors than Gibbs free energy, where anharmonic contributions to the entropic term may not be negligible.[47,48]

Theoretical Workflow Assessment. To assess the theoretical workflow, it was initially tested on 11 monomeric PFCA ions (C_6−C_{14}, C_{16} and C_{18}), whose conformations could be compared with those reported in the literature.[38,43,49−51] For the comparison between the experimental and theoretical CCS values, the CCS values obtained in DTIM served as the reference, as they did not differ notably (within ±2% error) from the CCS values obtained in TIMS or TWIMS. The assessment did not focus on the conformer generation process, as it differs between dimers and monomers. Instead, the primary validation centered on evaluating the level of theory applied for conformer optimization and energy calculations, as well as the parameters used for theoretical CCS calculations.

Therefore, for certain monomeric ions (C_6, C_9, C_{12} and C_{16}), the eight lowest energy conformers were additionally reoptimized with two other functionals that account for dispersion effects: CAM-B3LYP and WB97XD. Furthermore, the 6-311++G(d,p) basis set was also tested with the M06-2X functionals. The main results for monomeric ions were that the M06-2X/6-31+G(d,p) level of theory provided a reliable starting point for geometry optimization (see Table S6 and Figure S4), with the 6-311++G(d,p) basis yielding comparable results. The CAM-B3LYP and WB97XD functionals were less accurate, tending to overestimate BW average CCS values for long-chain PFCA monomers.

The effect of charge descriptors on theoretical CCS calculations (Mulliken and NBO) was investigated, and the advantages of considering ion-quadrupole interactions were observed. Partial charge descriptors had little impact, but Mulliken descriptors performed slightly better. Including the ion-quadrupole potential for nitrogen in the TMLJ method proved necessary for PFCAs, leading to an 8−10% increase in the predicted CCS, improving agreement with experimental data.

Using the conformers reoptimized at the M06-2X/6-31+G(d,p) level of theory and employing Mulliken charge descriptors, 100%, 82% and 64% of BW average CCS values were predicted within 5%, 3% and 2% error margins, respectively. These results are comparable to those of machine learning tools specifically trained for PFAS. For instance, CCSP 2.0 predicts 70% of PFAS CCS within a 3% error margin,[20] while another model (RF-Rdkit)[52] achieves 95% of PFAS CCS predictions within an 8% error margin. In our study, the CCS deviations range from −3.6% (−5.2 Å^2) for PFHpA (C_7) to +2.4% (+5.8 Å^2) for PFODA (C_{18}). However, prediction accuracy could likely be improved by including a larger and more diverse set of conformers to reduce potential biases toward overly compact or extended structures. Nevertheless, the primary goal of this study was not to achieve the highest possible accuracy but rather to gain insights into plausible structures of PFCA ions. In this respect, the helical isomer was generally not the lowest-energy conformer, which is consistent with findings from a recent study[50] (see Figure S5−S8 for a representation of the conformer ensemble for C_6, C_9, C_{12} and C_{16} monomeric ions). For C_{11} PFCA (#FC = 10) and longer chains, the CCS value for the helical isomer (#6 in Figure S7 and #8 in Figure S8) exceeded the DTIM experimental value by more than 2%, suggesting that it is unlikely to be the dominant conformer in the IMS cell. Second, the lowest-energy conformer (#1 in Figure S5−S8) identified using the monomer workflow typically showed a CCS value with an error exceeding 2% compared to experimental results, indicating it may not represent the most probable structure under experimental conditions. This is probably because the global minimum energy conformer has not been identified. To obtain plausible structural representations, the conformers with the lowest energy among those whose CCS value lies within a 2% error margin were selected and reported (see Figure S9). These conformers have an energy no more than 0.6 kcal/mol higher than that of the lowest-energy conformer, making them relevant for further analysis. A similar pattern is observed for all monomeric PFCA ions (Figure S9): the first two or three F−C−C−F dihedrals are typically less than 70−80°, causing the CO_2 moiety to curve toward the fluorinated chains. This behavior is consistent with the low-energy conformers reported in the literature,[43,49−51] and such chain bends can be attributed to C−F···C = O[53] or C−F···O=C[51] stabilizing hyperconjugative[54−56] interactions. For example, in the least energetic conformers of C_6 PFCA, second-order perturbation theory shows that negative hyperconjugation occurs between the lone pair of an oxygen atom (donor orbital) and an antibonding σ^*_{C-F} orbital (acceptor orbital). This interaction is possible if a fluorine atom is at a 2.70−2.75 Å distance from the O atom. Other hyperconjugation can also occur between bonding σ_{C-O} orbitals (donor) and antibonding σ^*_{C-F} orbitals (acceptor).

Despite these local bends, the overall shape remains approximately cylindrical, though with a slight "ball-cylinder" shape (Figure S10), where the length of the cylinder increases while the diameter remains nearly constant, and the "ball" size may slightly vary with chain length. This shape is still consistent with the linear CCS-m/z trendline.[29]

Thus, the chosen level of theory for the PFCA monomeric ions for geometry optimization and energy calculations, along with the CCS calculation parameters, are appropriate and reliable. Therefore, we can apply the same workflow to calculate the CCS values for dimeric ions.

https://doi.org/10.1021/jasms.5c00007
J. Am. Soc. Mass Spectrom. XXXX, XXX, XXX−XXX

Results for PFCA Symmetrical Dimeric Ions. For the symmetrical dimeric ions, an initial observation can be made regarding the 15 initial geometries. When optimized at the M06-2X/6-31+G(d,p) level of theory, some geometries resulted in extended structures where the two fluorinated chains were positioned opposite each other, while others formed compact structures with the fluorinated chains parallel and in close proximity (see Figure S11 for the C_9-C_9 dimer). Notably, as the chain lengths increased in these dimers, the Boltzmann weight of the parallel structures also increased. For example, it was 2% for the C_4-C_4 dimer, 20% for the C_9-C_9 dimer and 98% for the $C_{16}-C_{16}$ dimer. This trend may be linked to the fact that the increase in the chain length provides more opportunities for stabilizing C−F···F−C interactions involving a three-point motif.[55] These interactions are thought to play an important role in the van der Waals forces between fluorinated chains.[57] However, when only the 15 initial geometries are considered for CCS calculations using Mulliken descriptors, the BW average CCS value was found to be 3−11% higher than the experimental value, although the theoretical CCS trendline resembles the experimental trendline (see Figure S12). Furthermore, if parallel conformations are excluded from the BW CCS calculations, the resulting trendline becomes nearly linear (see Figure S12). This initial observation suggests that the overall structure of dimers may vary with increasing chain length, with longer-chain dimers being more likely to adopt a parallel conformation. This hypothesis is further supported by the fact that the experimental CCS of a dimeric ion is around 41−46% higher than that of its corresponding monomeric ion, rather than double its CCS value. Consequently, a parallel conformation of the two fluorinated chains in the dimer (#3 in Figure S11) appears more likely than an opposite conformation (#1 in Figure S11).

As the BW average CCS values calculated based on the 15 initial geometries were overestimated, relaxed potential energy scans were performed. In the monomeric ions, the dihedral angle closest to the carboxyl group had the greatest impact on conformer energy. Therefore, to save computational time, only the first two F−C−C−F dihedrals were scanned in one of the two fluorinated chains of the dimeric ions. Conformer selection and reoptimization were conducted as previously described (Figure 4), using the M06-2X/6-31+G(d,p) level of theory, to calculate the final BW average CCS values (black dots in Figure 5 and Table S7). For some dimers, CAM-B3LYP and WB97XD functionals were tested to reoptimize the same ten lowest-energy conformers identified using the M06-2X/6-31+G(d,p) method. However, these functionals overestimated the CCS values (data not shown) and were therefore discarded. Conversely, reoptimizing the ten lowest-energy conformers with the M06-2X functional and the 6-311++G(d,p) basis set produced promising results and were subsequently applied to all dimers (blue dots in Figure 5 and Table S7).

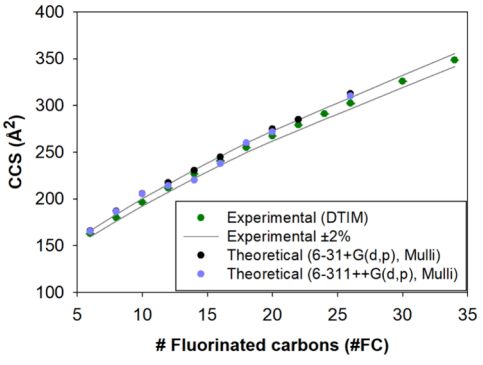

Figure 5. Comparison of theoretical Boltzmann-weighted average CCS values for PFCA homodimeric ions, calculated using conformers optimized using the M06-2X functional and Mulliken charge descriptors, with experimental CCS values.

For all dimers (C_4-C_4 to $C_{18}-C_{18}$) except one ($C_{16}-C_{16}$ or $C_{18}-C_{18}$), the workflow developed provided BW average CCS values within a 5% error margin. This was achieved using the M06-2X functional (with either the 6-31+G(d,p) or 6-311++G(d,p) basis sets) for conformer optimization and energy ranking, combined with Mulliken or NBO partial charge descriptors for CCS calculations. Notably, the combination of the 6-311++G(d,p) basis set and Mulliken charge descriptors yielded 38% of the CCS values falling within a 2% error margin and 62% within 3% error margin. The error ranged from −2.89% (−6.56 Å^2) for C_7-C_7 dimer to +5.82% (+ 18.97 Å^2) for $C_{16}-C_{16}$ dimer. This outcome is consistent with expectations, as the 6-311++G(d,p) basis set, being a triple-ζ basis set, is likely to reduce errors in structural optimization and energy ranking.[47] In addition, Mulliken charge descriptors were used to optimize the L-J parameters in the IMoS software,[58] and it is recommended to use partial charges consistent with those used for the parametrization.[35] Although achieving higher accuracy would be ideal for predictive purposes, the results obtained with the developed workflow are acceptable given the complexity of the system.

Additionally, considering that the machine learning protocol, trained specifically on PFAS, provides 70% of CCS predictions within a 3% error margin for monomeric PFAS ions[20] (which are less complex than the more flexible dimeric ions), the results of this study are satisfactory. These predictions could likely be improved by considering a broader and more diverse set of conformers, which would help avoid biases toward overly compact or extended structures. However, for the purposes of this study, the prediction performance is deemed sufficient. As with the monomeric ions, the primary purpose of this study was to identify plausible structures for the dimeric ions. To achieve this, the lowest-energy conformers among those whose CCS value fell within a 2% error margin were selected. This analysis was based on the structures and energies of conformers optimized with the 6-311++G(d,p) basis set and CCS values calculated using Mulliken charge descriptors. The selected conformers are presented in Figure 6, with additional data, including their BW percentage, CCS error percentage using both Mulliken and NBO charge descriptors, CF_3-CF_3 distances, and dipole moments, provided in Figure S13. These conformers are at most 1 kcal/mol higher in energy than the lowest-energy conformer. The structure displayed in Figure 6 for the $C_{16}-C_{16}$ and $C_{18}-C_{18}$ dimers corresponds to the structures with the lowest CCS error, although the errors exceed 2% when using Mulliken charge descriptors (+4.42% for $C_{16}-C_{16}$ and +4.00% for $C_{18}-C_{18}$). However, these errors are reduced when employing NBO charge descriptors (+0.86% for $C_{16}-C_{16}$ and +2.33% for $C_{18}-C_{18}$), making these structures still plausible.

In Figure 6, a pattern emerges where either the two fluorinated chains are closely aligned or one chain bents near its CO_2, curving toward the other CO_2 group and fluorinated chain. A noticeable difference in the general pattern occurs

https://doi.org/10.1021/jasms.5c00007
J. Am. Soc. Mass Spectrom. XXXX, XXX, XXX−XXX

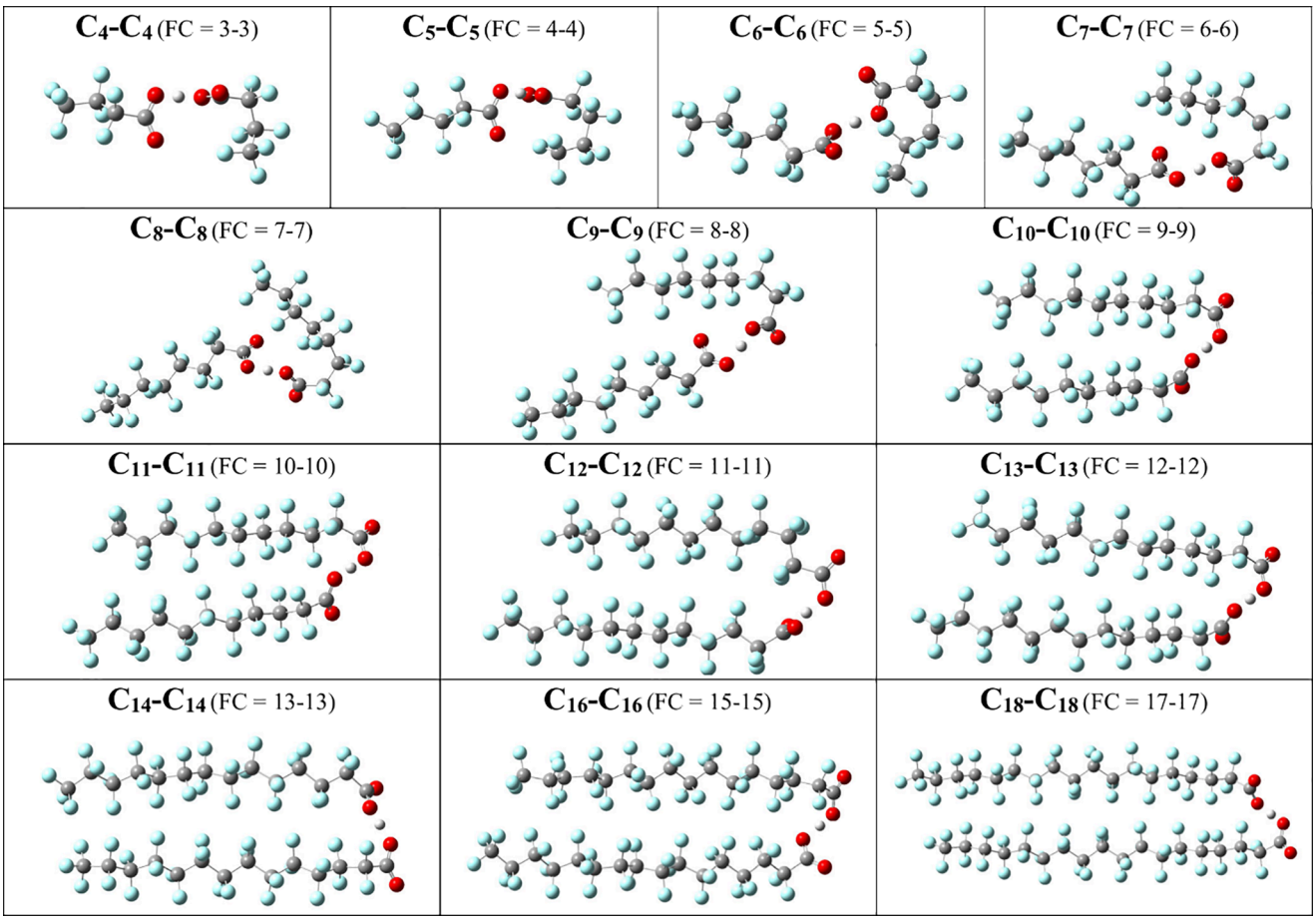

Figure 6. Structure of the lowest-energy conformer for each PFCA homodimeric ion, with a calculated CCS within 2% of DTIM experimental values (except for C_{16}−C_{16} and C_{18}−C_{18}), obtained at the M06-2X/6-311++G(d,p) level of theory.

between the C_9−C_9 and C_{10}−C_{10} dimers transitioning from structures with a bent chain to those with straight chains. This shift can be attributed to the fact that beyond a certain fluorinated chain length (9 FC in this case), additional intermolecular F−C···F−C interactions can occur, favoring a parallel orientation of the chains in the dimers.[4] However, for the C_9−C_9 dimers and shorter chains, second order perturbation theory suggests that the dominant intermolecular interactions, aside from hydrogen bonding, are C−F···O=C interactions, with minor contributions from F−C···C−F interactions. These interactions likely explain the bending observed near one CO_2 moiety. This behavior aligns with the initial observation from the 15 initial geometries and is also similar to the results obtained using the 6-31+G(d,p)/Mulliken method (Figure S14), where parallel conformations become predominant starting from the C_{12}−C_{12} dimer. Additionally, a relatively high error in BW average CCS was observed for the C_5−C_5 and C_6−C_6 dimer (+3.56% and +4.56%, respectively, see Table S7). This discrepancy can be attributed to their greater flexibility compared to the larger dimers. Indeed, the energy difference between compact and extended conformers in these smaller dimers is relatively low, which may lead to an overestimation of the BW of the extended conformers and, consequently, an overestimation of the BW average CCS value. This flexibility may also explain the relatively higher standard deviation observed in the experimental CCS values for these shorter-chain PFCA dimers (Table S4). The flexibility of the dimers can be further explored by examining the structures of the ten lowest-energy conformers, which are shown for some dimers in Figure S15−S20.

Thus, the workflow (Figure 4) employing the M062X/6-311++G(d,p) level of theory and Mulliken descriptors for CCS predictions provided reasonably accurate BW average CCS values for PFCA homodimeric ions. Furthermore, the structural analysis suggests that, in their dimeric form, the fluorinated chains are in close proximity which may contribute to their relative stability within the IMS cell.

Results for PFCA Asymmetrical Isomeric Dimeric Ions. For the isomeric dimeric ions, 6-31+G(d,p) and 6-311++G(d,p) basis sets were used with M06-2X functionals to optimize and rank the ten lowest-energy conformers. The BW CCS values calculated using the Mulliken charge description were all within a 2% error margin. However, the trendline showed slightly better consistency using 6-311++G(d,p) basis set (Figure 7, see Table S8). The structure of the lowest-energy conformers, optimized at the M06-2X/6-311++G(d,p) level of theory with CCS values within a 2% error margin, are presented in Figure 8 for all asymmetrical dimers. These structures are at most 0.9 kcal/mol higher in energy than the lowest energy conformer. Additional details are provided in Figure S21, and these structures can be compared to those obtained with the 6-31+G(d,p) basis set in Figure S22. Furthermore, the conformer sets of the C_2−C_{16}, C_6−C_{12} and C_9−C_9 dimers are available in Figure S23−S25.

In Figure 8, a similar structural pattern is observed for all dimers, where the longer chain bends near its CO_2 moiety

https://doi.org/10.1021/jasms.5c00007
J. Am. Soc. Mass Spectrom. XXXX, XXX, XXX−XXX

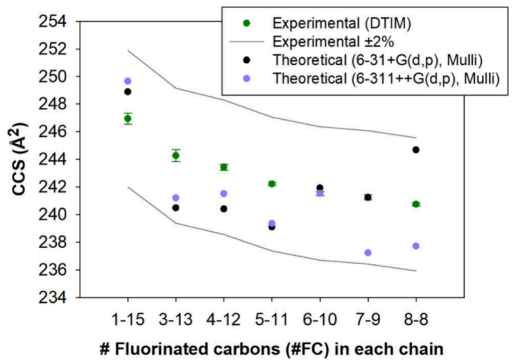

Figure 7. Comparison of theoretical Boltzmann-weighted CCS values for PFCA asymmetrical dimeric ions, calculated using conformers optimized using the M06-2X functional and Mulliken charge descriptors, with experimental CCS values.

toward the other chain. These structures likely result from a combination of stabilizing intra- and intermolecular F−C···C−F and C−F···O=C interactions. These conformations are consistent with the initial assumption that the overall shape is V-shaped. It suggests that the CCS values of the C_2-C_{16}; C_4-C_{14} and C_5-C_{13} dimers are influenced by the larger chain in each dimer, explaining their noticeably different CCS values. In contrast, the C_6-C_{12} dimer and other more symmetric dimers exhibit similar compactness, leading to similar CCS values. From this analysis of asymmetrical isomeric PFCA dimers, one can conclude that the workflow developed provides coherent BW CCS values and, more importantly, valuable structural insights. However, accurately predicting the small CCS differences between different isomeric dimers, such as the 2.5% difference observed between the C_2-C_{16} and C_9-C_9 dimers, remains a challenge. This raises questions about the workflow's ability to reliably predict CCS differences between isomers. To address this issue, further testing of less complex ions, such as monomeric PFCA isomers, would be useful. Enhancing predictive accuracy for dimers or monomers may require expanding the conformer set used for BW CCS predictions and developing a more systematic approach to conformer generation, particularly for the relatively flexible dimeric ions.

CONCLUSIONS

This study demonstrated that PFCA dimeric ions could be identified using three different IMS setups: DTIM, TIMS and TWIMS. The finding suggest that dimer formation is primarly influenced by the intrinsic properties of these compounds rather than the IMS setup used. Additionnaly, the CCS values for monomeric and dimeric PFCA ions were consistent across the three systems, falling within a tolerance range of ±2%, thereby confirming the reproducibility of measurements across different setups. This consistency also implies that the structures of these ions remain largely unaffected by the specific IMS device employed.

The theoretical CCS prediction workflow developed in this study is able to generate a set of conformers and calculate Boltzmann-weighted average CCS values within 5% error for both monomeric and dimeric PFCA ions. By utilizing M06-2X functionals with 6-31+G(d,p) or 6-311++G(d,p) basis sets for conformer optimization and energy ranking, and employing the trajectory method including 4−6−12 potentials and ion-quadrupole potentials for N_2, the Boltzmann-weighted CCS values obtained were within a 5% error margin. This can be likely improved by increasing the conformer set used to calculate the BW average CCS. More importantly, this approach revealed plausible structural conformations for

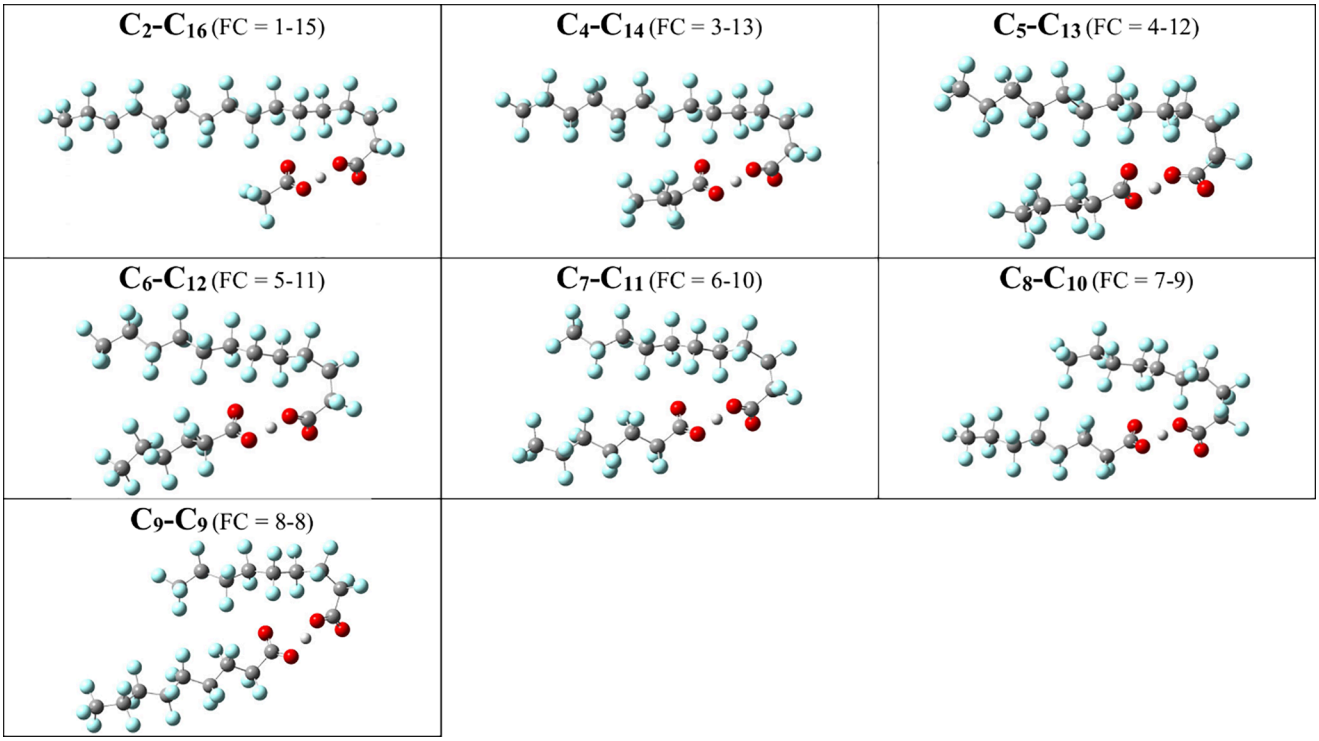

Figure 8. Structure of the lowest-energy conformer for each PFCA asymmetrical isomeric dimeric ion, with a calculated CCS within 2% of DTIM experimental values, obtained at the M06-2X/6-311++G(d,p) level of theory.

https://doi.org/10.1021/jasms.5c00007
J. Am. Soc. Mass Spectrom. XXXX, XXX, XXX−XXX

these ions, based on their low-energy and predicted CCS values close (within ±2%) to the DTIM experimental CCS value. The findings suggest that, in the monomeric form, the CO_2 moiety curves toward the fluorinated chain, while in the dimeric form, the fluorinated chains are likely in close proximity, especially for the dimers with the longer fluorinated chains, which may account for their relative stability within the IMS cell. This raises an interesting question about whether these fluorinated chains remain close when dimers are formed with larger cations, such as Na^+ or K^+. CCS calculations with these cations will assess whether the developed workflow and the proposed ion structures remain valid. A more chemically relevant charge descriptor, such as Merz−Singh−Kollman, could also be tested to validate the proposed structures. Finally, other carboxylated PFAS (e.g., perfluoroether carboxylic acids (PFECAs)) could be studied in IMS to asses their potential for dimerization and investigation into their conformation could be valuable, particularly to assess the impact of oxygen atoms within their fluorinated chains on the overall dimer structure. Finally, the workflow developed in this study could be tested on isomeric PFCAs (both monomers or dimers) to evaluate its ability to predict CCS differences between isomeric compounds.

■ ASSOCIATED CONTENT

Supporting Information

The Supporting Information is available free of charge at https://pubs.acs.org/doi/10.1021/jasms.5c00007.

Additional DTIM, TIMS and TWIMS settings; CCS calibration procedure; Experimental CCS values; Percentage error between theoretical BW CCS values and experimental values; Schematic representation of the shapes discussed with the CCS trendlines; Structure of the 15 initial geometries used in the C_2−C_{16} dimer example; Structures of the lowest energy conformers with a CCS within 2% error obtained using M06-2X/6-31+G(d,p) for the monomeric ion; Structures of the lowest energy conformers with a CCS within 2% error obtained using M06-2X/6-31+G(d,p) and M06-2X/6-311++G(d,p) levels of theory for the dimeric ions; Structures of the eight lowest energy conformers optimized at the M06-2X/6-31+G(d,p) level of theory for C_6, C_9, C_{12} and C_{16} monomeric ions; Structures of the ten lowest energy conformers optimized at the M06-2X/6-311++G(d,p) level of theory for C_4−C_4, C_6−C_6, C_{10}−C_{10}, C_{14}−C_{14} and C_{18}−C_{18} dimers as well as C_2−C_{16}, C_6−C_{12} and C_9−C_9 dimers (PDF)

■ AUTHOR INFORMATION

Corresponding Author

Gauthier Eppe − *Mass Spectrometry Laboratory, MolSys Research Unit, Chemistry Department, University of Liège, Liège 4000, Belgium;* orcid.org/0000-0002-4821-3115; Email: g.eppe@uliege.be

Authors

Aurore Schneiders − *Mass Spectrometry Laboratory, MolSys Research Unit, Chemistry Department, University of Liège, Liège 4000, Belgium;* orcid.org/0009-0005-1268-3632

Johann Far − *Mass Spectrometry Laboratory, MolSys Research Unit, Chemistry Department, University of Liège, Liège 4000, Belgium;* orcid.org/0000-0003-1208-6262

Lidia Belova − *Toxicological Centre, University of Antwerp, 2610 Wilrijk, Belgium;* orcid.org/0000-0001-7147-384X

Allison Fry − *Department of Chemistry, University of North Carolina at Chapel Hill, Chapel Hill, North Carolina 27599, United States*

Adrian Covaci − *Toxicological Centre, University of Antwerp, 2610 Wilrijk, Belgium;* orcid.org/0000-0003-0527-1136

Erin S. Baker − *Department of Chemistry, University of North Carolina at Chapel Hill, Chapel Hill, North Carolina 27599, United States;* orcid.org/0000-0001-5246-2213

Edwin De Pauw − *Mass Spectrometry Laboratory, MolSys Research Unit, Chemistry Department, University of Liège, Liège 4000, Belgium;* orcid.org/0000-0003-3475-1315

Complete contact information is available at: https://pubs.acs.org/10.1021/jasms.5c00007

Author Contributions

The authors confirm contribution to the paper as follows: study conception and design: A.S., J.F., E.D.P., G.E.; data collection: A.S., L.B.; implementation of the CCS prediction workflow: A.S. with input from J.F., E.D.P., G.E., A.F., E.S.B.; analysis and interpretation of results: A.S., J.F., E.D.P., G.E., L.B., A.C., A.F., E.S.B.; draft manuscript conception: A.S.; funding acquisition: G.E. All authors have given approval to the final version of the manuscript.

Notes

The authors declare no competing financial interest.

■ ACKNOWLEDGMENTS

Computational resources for Gaussian calculations have been provided by the Consortium des Équipements de Calcul Intensif (CÉCI), funded by the Fonds de la Recherche Scientifique de Belgique (F.R.S.-FNRS) under Grant No. 2.5020.11 and by the Walloon Region. A.S. also acknowledges financial support from the F.R.S.-FNRS (Research Fellow fellowship, 1.A.465.24F). L.B. acknowledges funding through a Research Foundation Flanders (FWO) fellowship (11G1821N). A.F and E.S.B. would also like to acknowledge funding from the NIH National Institute of Environmental Health Sciences (P42 ES027704) and a cooperative agreement with the Environmental Protection Agency (STAR RD 84003201). Analytical standards were purchased with funding from the Federal Public Service for Public Health, Food Chain Safety and Environment, as part of the RT23/07 PFASFORWARD project.

■ REFERENCES

(1) Wang, Z.; Buser, A. M.; Cousins, I. T.; Demattio, S.; Drost, W.; Johansson, O.; Ohno, K.; Patlewicz, G.; Richard, A. M.; Walker, G. W.; White, G. S.; Leinala, E. A New OECD Definition for Per- and Polyfluoroalkyl Substances. *Environ. Sci. Technol.* **2021**, *55* (23), 15575−15578.

(2) Buck, R. C.; Franklin, J.; Berger, U.; Conder, J. M.; Cousins, I. T.; de Voogt, P.; Jensen, A. A.; Kannan, K.; Mabury, S. A.; van Leeuwen, S. P. J. Perfluoroalkyl and Polyfluoroalkyl Substances in the Environment: Terminology, Classification, and Origins. *Integr. Environ. Assess. Manag.* **2011**, *7* (4), 513−541.

(3) Teymourian, T.; Teymoorian, T.; Kowsari, E.; Ramakrishna, S. A Review of Emerging PFAS Contaminants: Sources, Fate, Health Risks, and a Comprehensive Assortment of Recent Sorbents for PFAS Treatment by Evaluating Their Mechanism. *Res. Chem. Intermed.* **2021**, *47*, 4879−4914.

(4) Hasegawa, T. Physicochemical Nature of Perfluoroalkyl Compounds Induced by Fluorine. *Chem. Rec.* **2017**, *17* (10), 903–917.
(5) Grandjean, P.; Clapp, R. Perfluorinated Alkyl Substances: Emerging Insights into Health Risks. *New Solut.* **2015**, *25* (2), 147–163.
(6) *Listing of POPs in the Stockholm Convention*. http://www.pops.int/TheConvention/ThePOPs/AllPOPs/tabid/2509/Default.aspx (accessed 2024–08–01).
(7) Interstate technology & regulatory council. *PFAS Fact Sheet on History and Use*. https://pfas-1.itrcweb.org/wp-content/uploads/2023/10/HistoryandUse_PFAS_Fact-Sheet_Sept2023_final.pdf (accessed 2024–08–01).
(8) Schymanski, E. L.; Zhang, J.; Thiessen, P. A.; Chirsir, P.; Kondic, T.; Bolton, E. E. Per- and Polyfluoroalkyl Substances (PFAS) in PubChem: 7 Million and Growing. *Environ. Sci. Technol.* **2023**, *57* (44), 16918–16928.
(9) Gao, K.; Chen, Y.; Xue, Q.; Fu, J.; Fu, K.; Fu, J.; Zhang, A.; Cai, Z.; Jiang, G. Trends and Perspectives in Per-and Polyfluorinated Alkyl Substances (PFAS) Determination: Faster and Broader. *TrAC - Trends Anal. Chem.* **2020**, *133*, 116114.
(10) Pan, Y.; Wang, J.; Yeung, L. W. Y.; Wei, S.; Dai, J. Analysis of Emerging Per- and Polyfluoroalkyl Substances: Progress and Current Issues. *TrAC - Trends Anal. Chem.* **2020**, *124*, 115481.
(11) Wang, Z.; Cousins, I. T.; Scheringer, M.; Hungerbuehler, K. Hazard Assessment of Fluorinated Alternatives to Long-Chain Perfluoroalkyl Acids (PFAAs) and Their Precursors: Status Quo, Ongoing Challenges and Possible Solutions. *Environ. Int.* **2015**, *75*, 172–179.
(12) Steeves, K.; Cahill, L. S.; Jobst, K. J. Emerging Perfluoroalkyl Substances in Environmental Waters Revealed by Non-Targeted Screening. *Curr. Opin. Environ. Sci. Health* **2024**, *37*, 100531.
(13) Liu, Y.; D'Agostino, L. A.; Qu, G.; Jiang, G.; Martin, J. W. High-Resolution Mass Spectrometry (HRMS) Methods for Non-target Discovery and Characterization of Poly- and per-Fluoroalkyl Substances (PFAS) in Environmental and Human Samples. *TrAC - Trends Anal. Chem.* **2019**, *121*, 115420.
(14) Dodds, J. N.; Hopkins, Z. R.; Knappe, D. R. U.; Baker, E. S. Rapid Characterization of Per- And Polyfluoroalkyl Substances (PFAS) by Ion Mobility Spectrometry-Mass Spectrometry (IMS-MS). *Anal. Chem.* **2020**, *92* (6), 4427–4435.
(15) Kirkwood, K. I.; Fleming, J.; Nguyen, H.; Reif, D. M.; Baker, E. S.; Belcher, S. M. Utilizing Pine Needles to Temporally and Spatially Profile Per- and Polyfluoroalkyl Substances (PFAS). *Environ. Sci. Technol.* **2022**, *56* (6), 3441–3451.
(16) Ahmed, E.; Mohibul Kabir, K. M.; Wang, H.; Xiao, D.; Fletcher, J.; Donald, W. A. Rapid Separation of Isomeric Perfluoroalkyl Substances by High-Resolution Differential Ion Mobility Mass Spectrometry. *Anal. Chim. Acta* **2019**, *1058*, 127–135.
(17) D'Atri, V.; Causon, T.; Hernandez-Alba, O.; Mutabazi, A.; Veuthey, J. L.; Cianferani, S.; Guillarme, D. Adding a New Separation Dimension to MS and LC–MS: What Is the Utility of Ion Mobility Spectrometry? *J. Sep. Sci.* **2018**, *41* (1), 20–67.
(18) Gabelica, V. CHAPTER 1: Ion Mobility–Mass Spectrometry: an Overview. *Ion Mobility-Mass Spectrometry: Fundamentals and Applications* **2021**, 1–25.
(19) Gabelica, V.; Marklund, E. Fundamentals of Ion Mobility Spectrometry. *Curr. Opin. Chem. Biol.* **2018**, *42*, 51–59.
(20) Foster, M.; Rainey, M.; Watson, C.; Dodds, J. N.; Kirkwood, K. I.; Fernández, F. M.; Baker, E. S. Uncovering PFAS and Other Xenobiotics in the Dark Metabolome Using Ion Mobility Spectrometry, Mass Defect Analysis, and Machine Learning. *Environ. Sci. Technol.* **2022**, *56* (12), 9133–9143.
(21) Belova, L.; Caballero-Casero, N.; Van Nuijs, A. L. N.; Covaci, A. Ion Mobility-High-Resolution Mass Spectrometry (IM-HRMS) for the Analysis of Contaminants of Emerging Concern (CECs): Database Compilation and Application to Urine Samples. *Anal. Chem.* **2021**, *93* (16), 6428–6436.
(22) Valdiviezo, A.; Aly, N. A.; Luo, Y. S.; Cordova, A.; Casillas, G.; Foster, M. K.; Baker, E. S.; Rusyn, I. Analysis of Per- and Polyfluoroalkyl Substances in Houston Ship Channel and Galveston Bay Following a Large-Scale Industrial Fire Using Ion-Mobility-Spectrometry-Mass Spectrometry. *J. Environ. Sci. (China)* **2022**, *115*, 350–362.
(23) Vera, P.; Canellas, E.; Dreolin, N.; Goshawk, J.; Nerín, C. The Analysis of the Migration of per and Poly Fluoroalkyl Substances (PFAS) from Food Contact Materials Using Ultrahigh Performance Liquid Chromatography Coupled to Ion-Mobility Quadrupole Time-of-Flight Mass Spectrometry (UPLC- IMS-QTOF). *Talanta* **2024**, *266*, 124999.
(24) Díaz-Galiano, F. J.; Murcia-Morales, M.; Monteau, F.; Le Bizec, B.; Dervilly, G. Collision Cross-Section as a Universal Molecular Descriptor in the Analysis of PFAS and Use of Ion Mobility Spectrum Filtering for Improved Analytical Sensitivities. *Anal. Chim. Acta* **2023**, *1251*, 341026.
(25) Cheng, J.; Psillakis, E.; Hoffmann, M. R.; Colussi, A. J. Acid Dissociation versus Molecular Association of Perfluoroalkyl Oxoacids: Environmental Implications. *J. Phys. Chem. A* **2009**, *113* (29), 8152–8156.
(26) Cai, W.; Navarro, D. A.; Du, J.; Ying, G.; Yang, B.; McLaughlin, M. J.; Kookana, R. S. Increasing Ionic Strength and Valency of Cations Enhance Sorption through Hydrophobic Interactions of PFAS with Soil Surfaces. *Sci. Total Environ.* **2022**, *817*, 152975.
(27) Shen, Z.; Ge, J.; Ye, H.; Tang, S.; Li, Y. Cholesterol-like Condensing Effect of Perfluoroalkyl Substances on a Phospholipid Bilayer. *J. Phys. Chem. B* **2020**, *124* (26), 5415–5425.
(28) Frisch, M. J.; Trucks, G. W.; Schlegel, H. B.; Scuseria, G. E.; Robb, M. A.; Cheeseman, J. R.; Scalmani, G.; Barone, V.; Petersson, G. A.; Nakatsuji, H.; Li, X.; Caricato, M.; Marenich, A. V.; Bloino, J.; Janesko, B. G.; Gomperts, R.; Mennucci, B.; Hratchian, H. P.; Ortiz, J. V.; Izmaylov, A. F.; Sonnenberg, J. L.; Williams-Young, D.; Ding, F.; Lipparini, F.; Egidi, F.; Goings, J.; Peng, B.; Petrone, A.; Henderson, T.; Ranasinghe, D.; Zakrzewski, V. G.; Gao, J.; Rega, N.; Zheng, G.; Liang, W.; Hada, M.; Ehara, M.; Toyota, K.; Fukuda, R.; Hasegawa, J.; Ishida, M.; Nakajima, T.; Honda, Y.; Kitao, O.; Nakai, H.; Vreven, T.; Throssell, K.; Montgomery, J. A., Jr.; Peralta, J. E.; Ogliaro, F.; Bearpark, M. J.; Heyd, J. J.; Brothers, E. N.; Kudin, K. N.; Staroverov, V. N.; Keith, T. A.; Kobayashi, R.; Normand, J.; Raghavachari, K.; Rendell, A. P.; Burant, J. C.; Iyengar, S. S.; Tomasi, J.; Cossi, M.; Millam, J. M.; Klene, M.; Adamo, C.; Cammi, R.; Ochterski, J. W.; Martin, R. L.; Morokuma, K.; Farkas, O.; Foresman, J. B.; Fox, D. J. *Gaussian 16*, Revision C.01; Gaussian, Inc.: Wallingford CT, 2016.
(29) Larriba, C.; Hogan, C. J. Ion Mobilities in Diatomic Gases: Measurement versus Prediction with Non-Specular Scattering Models. *J. Phys. Chem. A* **2013**, *117* (19), 3887–3901.
(30) Kim, H.; Kim, H. I.; Johnson, P. V.; Beegle, L. W.; Beauchamp, J. L.; Goddard, W. A.; Kanik, I. Experimental and Theoretical Investigation into the Correlation between Mass and Ion Mobility for Choline and Other Ammonium Cations in N_2. *Anal. Chem.* **2008**, *80* (6), 1928–1936.
(31) Gabelica, V.; Shvartsburg, A. A.; Afonso, C.; Barran, P.; Benesch, J. L. P.; Bleiholder, C.; Bowers, M. T.; Bilbao, A.; Bush, M. F.; Campbell, J. L.; Campuzano, I. D. G.; Causon, T.; Clowers, B. H.; Creaser, C. S.; De Pauw, E.; Far, J.; Fernandez-Lima, F.; Fjeldsted, J. C.; Giles, K.; Groessl, M.; Hogan, C. J.; Hann, S.; Kim, H. I.; Kurulugama, R. T.; May, J. C.; McLean, J. A.; Pagel, K.; Richardson, K.; Ridgeway, M. E.; Rosu, F.; Sobott, F.; Thalassinos, K.; Valentine, S. J.; Wyttenbach, T. Recommendations for reporting ion mobility Mass Spectrometry measurements. *Mass Spectrom Rev.* **2019**, *38* (3), 291–320.
(32) Haler, J. R. N.; Morsa, D.; Lecomte, P.; Jérôme, C.; Far, J.; De Pauw, E. Predicting Ion Mobility-Mass Spectrometry Trends of Polymers Using the Concept of Apparent Densities. *Methods* **2018**, *144*, 125–133.
(33) Haler, J. R. N.; Béchet, E.; Kune, C.; Far, J.; De Pauw, E. Geometric Analysis of Shapes in Ion Mobility-Mass Spectrometry. *J. Am. Soc. Mass Spectrom.* **2022**, *33* (2), 273–283.

https://doi.org/10.1021/jasms.5c00007
J. Am. Soc. Mass Spectrom. XXXX, XXX, XXX–XXX

(34) Colby, S. M.; Thomas, D. G.; Nuñez, J. R.; Baxter, D. J.; Glaesemann, K. R.; Brown, J. M.; Pirrung, M. A.; Govind, N.; Teeguarden, J. G.; Metz, T. O.; Renslow, R. S. ISiCLE: A Quantum Chemistry Pipeline for Establishing in Silico Collision Cross Section Libraries. *Anal. Chem.* **2019**, *91* (7), 4346−4356.
(35) Lee, J. W.; Lee, H. H. L.; Davidson, K. L.; Bush, M. F.; Kim, H. I. Structural Characterization of Small Molecular Ions by Ion Mobility Mass Spectrometry in Nitrogen Drift Gas: Improving the Accuracy of Trajectory Method Calculations. *Analyst* **2018**, *143* (8), 1786−1796.
(36) Nielson, F. F.; Colby, S. M.; Thomas, D. G.; Renslow, R. S.; Metz, T. O. Exploring the Impacts of Conformer Selection Methods on Ion Mobility Collision Cross Section Predictions. *Anal. Chem.* **2021**, *93* (8), 3830−3838.
(37) Das, S.; Dinpazhoh, L.; Tanemura, K. A.; Merz, K. M. Rapid and Automated *Ab Initio* Metabolite Collisional Cross Section Prediction from SMILES Input. *J. Chem. Inf. Model.* **2023**, *63* (16), 4995−5000.
(38) Rayne, S.; Forest, K. Comparative Semiempirical, Ab Initio, and Density Functional Theory Study on the Thermodynamic Properties of Linear and Branched Perfluoroalkyl Sulfonic Acids/Sulfonyl Fluorides, Perfluoroalkyl Carboxylic Acid/Acyl Fluorides, and Perhydroalkyl Sulfonic Acids, Alkanes, and Alcohols. *J. Mol. Struct. THEOCHEM* **2010**, *941* (1−3), 107−118.
(39) Stewart, J. J. P. Optimization of Parameters for Semiempirical Methods V: Modification of NDDO Approximations and Application to 70 Elements. *J. Mol. Model.* **2007**, *13* (12), 1173−1213.
(40) Zhao, Y.; Truhlar, D. G. The M06 Suite of Density Functionals for Main Group Thermochemistry, Thermochemical Kinetics, Noncovalent Interactions, Excited States, and Transition Elements: Two New Functionals and Systematic Testing of Four M06-Class Functionals and 12 Other Functionals. *Theor. Chem. Acc.* **2008**, *120* (1−3), 215−241.
(41) Hidalgo, A.; Giroday, T.; Mora-Diez, N. Thermodynamic Stability of Neutral and Anionic PFOAs. *Theor. Chem. Acc.* **2015**, *134* (11), 124.
(42) Giroday, T.; Montero-Campillo, M. M.; Mora-Diez, N. Thermodynamic Stability of PFOS: M06-2X and B3LYP Comparison. *Comput. Theor. Chem.* **2014**, *1046*, 81−92.
(43) Rayne, S.; Forest, K. Theoretical Studies on the pKa Values of Perfluoroalkyl Carboxylic Acids. *J. Mol. Struct. THEOCHEM* **2010**, *949* (1−3), 60−69.
(44) Larriba-Andaluz, C.; Prell, J. S. Fundamentals of Ion Mobility in the Free Molecular Regime. Interlacing the Past, Present and Future of Ion Mobility Calculations. *Int. Rev. Phys. Chem.* **2020**, *39* (4), 569−623.
(45) Larriba-Andaluz, C.; Fernández-García, J.; Ewing, M. A.; Hogan, C. J.; Clemmer, D. E. Gas Molecule Scattering & Ion Mobility Measurements for Organic Macro-Ions in He versus N_2 Environments. *Phys. Chem. Chem. Phys.* **2015**, *17* (22), 15019−15029.
(46) Stow, S. M.; Causon, T. J.; Zheng, X.; Kurulugama, R. T.; Mairinger, T.; May, J. C.; Rennie, E. E.; Baker, E. S.; Smith, R. D.; McLean, J. A.; Hann, S.; Fjeldsted, J. C. An Interlaboratory Evaluation of Drift Tube Ion Mobility−Mass Spectrometry Collision Cross Section Measurements. *Anal. Chem.* **2017**, *89* (17), 9048−9055.
(47) Bursch, M.; Mewes, J.; Hansen, A.; Grimme, S. Best-Practice DFT Protocols for Basic Molecular Computational Chemistry**. *Angew. Chem., Int. Ed.* **2022**, *61* (42), No. e202205735.
(48) Isayev, O.; Gorb, L.; Leszczynski, J. Theoretical Calculations: Can Gibbs Free Energy for Intermolecular Complexes Be Predicted Efficiently and Accurately? *J. Comput. Chem.* **2007**, *28* (9), 1598−1609.
(49) McTaggart, M.; Malardier-Jugroot, C. The Role of Helicity in PFAS Resistance to Degradation: DFT Simulation of Electron Capture and Defluorination. *Phys. Chem. Chem. Phys.* **2024**, *26* (5), 4692−4701.
(50) Lorpaiboon, W.; Ho, J. High-Level Quantum Chemical Prediction of C−F Bond Dissociation Energies of Perfluoroalkyl Substances. *J. Phys. Chem. A* **2023**, *127* (38), 7943−7953.
(51) Schilberg, R. N.; Wei, S.; Twagirayezu, S.; Neill, J. L. Conformational Dynamics of Perfluorooctanoic Acid (PFOA) Studied by Molecular Rotational Resonance (MRR) Spectroscopy. *Chem. Phys. Lett.* **2021**, *778*, 138789.
(52) Mu, H.; Yang, Z.; Chen, L.; Gu, C.; Ren, H.; Wu, B. Suspect and Nontarget Screening of Per- and Polyfluoroalkyl Substances Based on Ion Mobility Mass Spectrometry and Machine Learning Techniques. *J. Hazard. Mater.* **2024**, *461*, 132669.
(53) Cormanich, R. A.; Rittner, R.; O'Hagan, D.; Bühl, M. Inter- and Intramolecular CF···C = O Interactions on Aliphatic and Cyclohexane Carbonyl Derivatives. *J. Comput. Chem.* **2016**, *37* (1), 25−33.
(54) Cormanich, R. A.; O'Hagan, D.; Bühl, M. Hyperconjugation Is the Source of Helicity in Perfluorinated *n* -Alkanes. *Angew. Chem., Int. Ed.* **2017**, *56* (27), 7867−7870.
(55) Alabugin, I. V.; Dos Passos Gomes, G.; Abdo, M. A. Hyperconjugation. *WIREs Comput. Mol. Sci.* **2019**, *9* (2), No. e1389.
(56) Omorodion, H.; Twamley, B.; Platts, J. A.; Baker, R. J. Further Evidence on the Importance of Fluorous−Fluorous Interactions in Supramolecular Chemistry: A Combined Structural and Computational Study. *Cryst. Growth Des.* **2015**, *15* (6), 2835−2841.
(57) Hasegawa, T. Understanding of the Intrinsic Difference between Normal- and Perfluoro-Alkyl Compounds toward Total Understanding of Material Properties. *Chem. Phys. Lett.* **2015**, *627*, 64−66.
(58) Wu, T.; Derrick, J.; Nahin, M.; Chen, X.; Larriba-Andaluz, C. Optimization of Long-Range Potential Interaction Parameters in Ion Mobility Spectrometry. *J. Chem. Phys.* **2018**, *148* (7), No. 074102.

https://doi.org/10.1021/jasms.5c00007
J. Am. Soc. Mass Spectrom. XXXX, XXX, XXX−XXX